Tribol Lett (2014) 53:293–301
DOI 10.1007/s11249-013-0267-y

ORIGINAL PAPER

Arc Erosion Wear Characteristics and Mechanisms of Pure Carbon Strip Against Copper Under Arcing Conditions

Xianzhi Xiong · Chuanjun Tu · Ding Chen · Jianqi Zhang · Jianghua Chen

Received: 27 January 2013 / Accepted: 18 November 2013 / Published online: 10 December 2013

Abstract The wear behavior of pure carbon strip against copper (carbon/copper pair) under continuous arcing condition was investigated. To simulate the extreme condition of continuous arc discharge at high current, sliding wear tests were conducted on a home-made wear tester. The arc erosion wear characteristics and mechanisms of carbon/copper pair were studied by analyzing the wear scars and wear debris of the carbon strip in detail. Therefore, various analytical techniques, including Raman spectroscopy, transmission and scanning electron microscopy, and focused ion beam systems, were utilized to characterize the wear scars and wear debris of the carbon strip. The results show that the wear rate and the degree of arc erosion of the carbon strip increase with increasing electric current density. Typical entwined turbostratic carbon nanospheres (ETCNs) exhibited sphere-like stacking structure that were observed in the microstructure of the wear debris of the carbon strip produced during the friction process with current, which is the characteristic of the textural changes in carbon materials under combined arcing and sliding friction conditions. Moreover, the number and size of ETCNs increase with the electric current density increase. The arc erosion wear mechanisms of the carbon/copper pair are mainly due to the synergetic action of oxidation ablation, local electric arc impact and high-temperature graphitization under continuous arcing.

Keywords Carbon strip · Arc erosion wear · Microstructure · Entwined turbostratic carbon nanospheres · Wear mechanism

1 Introduction

High-speed electrified railways represent a continually developing trend in modern transportation all over the world [1, 2]. However, their running speed is mainly limited by the current collection quality of the pantograph–catenary system, vehicle technology and braking technology [3, 4]. The pantograph–catenary system is the key factor, because it has a direct influence on both the stable operation of trains and the service life of friction pairs. Arc erosion wear, one of the main sources of reduced performance, is mainly caused by off-line sliding or abnormal contact between contact strip and contact wire [5, 6], leading to serious damage to the worn surface of friction pairs since the local temperature rises and the oxidation of contact surfaces occurs. As the speed and load of a train increase, high-frequency arc erosion becomes more serious, and various wear behaviors are induced by the arc as the speed of a locomotive increases. Meanwhile, the wear characteristics of the contact interface will be directly modified.

To relieve the severe wear of contact strip caused by arc erosion due to the imperfect contact between friction pairs, over the past decades, a few scientists have performed studies on the wear behaviors and mechanisms of friction pairs under an electric current density. Matsuyama [7] investigated the tribological behavior of pantographs under an electric current and observed distinct arc ablation and melt phenomena during the electrical wear process in preliminary studies. Kubo and Kato [8, 9] systematically

Electronic supplementary material The online version of this article (doi:10.1007/s11249-013-0267-y) contains supplementary material, which is available to authorized users.

X. Xiong · C. Tu (✉) · D. Chen · J. Zhang · J. Chen
College of Materials Science and Engineering, Hunan University, Changsha 410082, People's Republic of China
e-mail: tcj@hnu.edu.cn

studied the effect of arc discharge on the wear rate of Cu-impregnated carbon strip in unlubricated sliding against Cu trolley wire under an electric current and discovered that the wear rate of the contact strip increased with the increasing electrical current. Moreover, the wear rate reached its maximum at an electrical current of 150 A and then decreased. The effect of mechanical, electrical and thermal parameters on the surface damage of electrical contact copper was investigated by Senouci et al. [10] around the same time. They found that the high current density in dynamical contact enhanced the oxidation process of the sliding surface and then induced an electric arc and copper damage. Sliding copper wire was damaged by abrasion, triboxidation and electric arc. Nagasawa and Kato [11] reported the wear mechanism of sliding copper alloy wire against iron-based strip under an electric current. The results showed that the wear rate of the contact wire was related to the heat generated at the contact interface of friction pairs by friction, thermal resistance and arcing, which originated from the off-line area between the contact strip and contact wire. In addition, Chen et al. [12] studied the arc erosion of a resin roasting strip sliding against copper and developed a model of the arc extinction of the friction pairs. Recently, comparisons between the wear behaviors due to an increase in temperature and arc discharge were made under the same testing conditions reported by Ding et al. [13]. Flash temperature accumulates on the friction couple because of the occurrence of arc discharge. The heat produced by Joule heat, arc discharge and friction results in a rapid rise in temperature of the friction couple. The severe wear of the carbon strip was mainly caused by arc erosion, abrasive wear and adhesive wear. In summary, major efforts have been devoted to investigating the wear behavior of carbon strip under an electrical current. Notable advances have been made in understanding the wear mechanisms under an electrical current. Moreover, it has been generally accepted that the wear loss increases with increasing electrical current and deduced that the severe wear of contact strip is mainly caused by arc erosion. However, many analyses and explanations of wear characteristics and mechanisms for friction pairs are barely based on the morphological changes in the worn surface with and without electric current. Seldom, research directs attention to the wear debris of the carbon strip. In this context, the wear mechanisms of contact strip sliding against contact wire under an electrical current are not clear, i.e., no reasonable explanations for the detailed arc erosion wear characteristics or mechanisms of friction pairs have been provided due to inadequate evidence.

In this study, a series of experiments were performed to study the wear behavior of a carbon/copper pair under continuous arcing conditions. The arc erosion wear characteristics were investigated in detail by scanning electron microscopy (SEM), Raman spectroscopy and transmission electron microscopy (TEM). Based on the SEM and TEM observations, a new arc erosion wear mechanism of the carbon/copper pair under continuous arcing conditions was proposed.

2 Experimental

A pure carbon strip used in high-speed trains was chosen as the test material. To conduct electrical sliding wear tests during the arc discharge process, the carbon strip was machined into the desired cylindrical shape with a cross-sectional area of 100 mm^2 and a height of 36 mm. Its chemical composition (wt%) mainly included 91.9 % C, 7.72 % O and 0.38 % S. The volume density of the carbon strip was 1.87 g/cm^3. A friction disk measuring 700 mm in diameter and 5 mm in width was made of pure copper; the disk was used for electrical sliding wear experiments with the carbon strip. The details of the experimental processes have been reported elsewhere [14].

Sliding wear tests under an electrical current were performed on a home-made wear tester to simulate train motion in air. A schematic illustration of this electrical wear test apparatus is shown in Fig. S1 (see Supplementary Material). A low voltage and high AC current generated by the power source flow from one contact strip to the copper disk and then to the other contact strip. The wear rate was defined as the wear mass loss of the carbon strip per unit length and unit load over one sliding pass. During testing, the selected values of the electric current density (electric current per unit area, $J = I/A$) were 0, 250, 375, 500 and 650 A/cm^2. The normal load on the carbon/copper pair was 60 N. The test performed under an applied electrical current lasted 300 s to ensure a state of continuous arc discharge for each experiment within the testing time on the home-made wear tester, which has groove structures on the copper disk surface. The linear velocity of the copper disk surface was determined to be 30.6 m/s. Prior to wear testing, all of the specimen surfaces were polished using 2000-grain abrasive paper first and then 5000-grain abrasive paper and cleaned with alcohol. The circle jumping degree was corrected prior to each experiment to ensure the rotation of the copper friction pair is the central axis. The wear debris was collected immediately below the carbon strip during the wear process.

The entire process of current-carrier friction was recorded by a digital camera (Canon IXUS310 HS), with which the influence of the strength of the arc was characterized qualitatively. In order to measure the weight of the strip before and after the test, an electronic balance with an accuracy of 0.0001 g was used. The morphologies and

microstructures of the wear scars and the wear debris of the carbon strip were observed by SEM (JEOL, JSM-6700F) and TEM (JEOL, JEM-3010). TEM specimens of the wear debris and carbon matrix were prepared using a FEI Nova 200 Nanolab DualBeam SEM/FIB system [15] along the edge of the wear debris. The graphitization degree of the wear scars of the carbon strip was studied by laser Raman spectroscopy (HR 800 Raman). All experiments were conducted at ambient temperature (25 ± 2 °C) and in 70–80 % relative humidity.

3 Results and Discussion

3.1 Effects of Electric Current Density on the Wear Rate of the Carbon Strip

Figure 1 shows the variation in the wear rate of the carbon strip with electrical current. A stable electric arc between the carbon/copper pair was observed by a digital camera during the wear process under an electric current (see Supplementary Material, Fig. S2).

As shown in Fig. 1, the wear rate of the carbon strip increases with increasing electric current density under a continuous arcing environment. The wear rate of the carbon strip increases rapidly under a low electric current density (<250 A/cm^2), gradually increases under intermediate electric current densities (250–500 A/cm^2) and then increases dramatically (>500 A/cm^2). The wear rate of the carbon strip under an electrical current is higher than that without an electrical current, and it increased with the increase in electric current density. Firstly, there are universal electric arc phenomena (see Supplementary Material, Fig. S2) observed between carbon/copper pairs under the current-carrying condition. The arc plasma temperature reaches 3,500–4,000 K [5, 16], which can cause carbon–carbon bonds to break. Thus, the carbon material in the areas of arc erosion would drop from the friction surface as the effect of oxidative ablation and sublimation under arc erosion, which is the main cause to the increase in the wear rate under the current-carrying condition [17]. In addition, with the increase in the current density, the intensity of the arc increased, which would enhance the effect of arc impact and result in an increase in the wear rate [17–19]. Secondly, the friction surface was under the comprehensive effect of three forms of heat generated in the wear process with current [11]: frictional heat, Joule heat and the arc heat, which would raise the temperature of the friction surface and thus degrade wear performance because of the oxidization of carbon materials [17]. In this way, the wear rate is increased. Moreover, the oxidation of the carbon strips in asperity contacts will be accelerated after increasing the current density, for the surface temperature is extremely high.

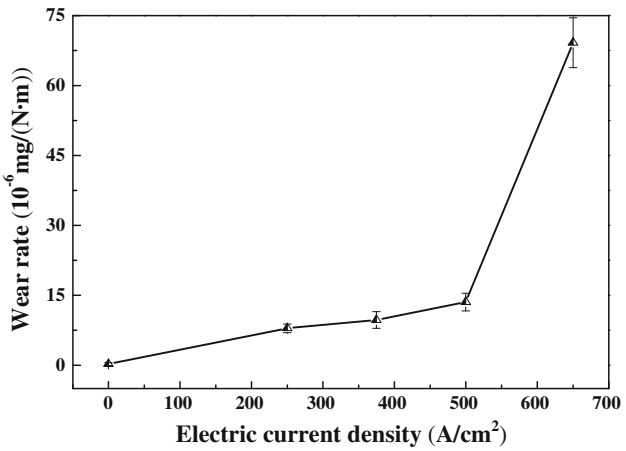

Fig. 1 Variation in the wear rate of carbon strip with electric current density

Figure 1 also suggests that the wear rate increases dramatically when the electric current density exceeds 500 A/cm^2. The wear rate of the carbon strip when the current density is 650 A/cm^2 (69.19×10^{-6} mg/(m N)) is approximately 288 times as much as that when the current density is 0 A/cm^2 [0.24×10^{-6} mg/(m N)]. It is mainly attributed to the rise in the contact surface temperature of the carbon strip caused by Joule heating and the high temperature instantly induced by arc discharge at high current density, which would even cause the overheating of the wear surface (see Supplementary Material, Fig. S2-d). Thus, the wear becomes severe when the contact area temperature exceeded the threshold temperature of C–C bond rupture and surface oxide layer spallation on contact interfaces. Meanwhile, the carbon material on the wear scar area was easily heated and sublimated or directly oxidized in an oxidizing atmosphere [8, 9].

3.2 Microstructure of the Wear Interface of Carbon Strip

3.2.1 Characterization of the Wear Scars

The SEM morphologies of the wear scars of carbon strip under electric current density of 0, 250, 375, 500 and 650 A/cm^2 are shown in Fig. 2. The arrow indicates the direction of relative movement of the carbon/copper pair.

As shown in Fig. 2, the wear scar features clearly varied with the applied current density. The SEM images of the wear scars show that the worn surfaces are dense and no obvious oxidation zone when the current density is 0 A/cm^2 (Fig. 2a). It is observed that there is a surface lubricant film with flake structure formed on the wear scars of carbon strip. However, Fig. 2b–e clearly shows many arc craters

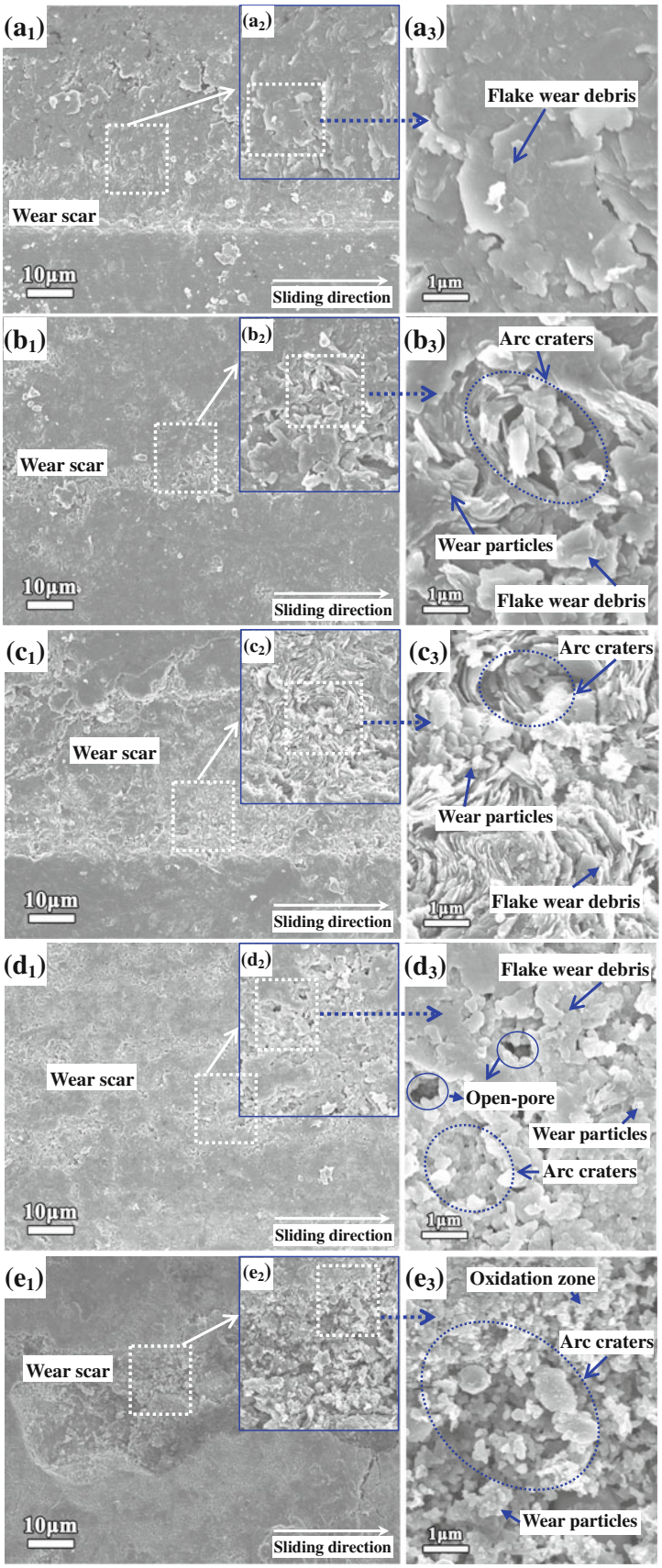

Fig. 2 SEM morphologies of the wear scars of carbon strip under electric current density: (a_1), (a_2), (a_3)—at $J = 0$ A/cm^2; (b_1), (b_2), (b_3)—at $J = 250$ A/cm^2; (c_1), (c_2), (c_3)—at $J = 375$ A/cm^2; (d_1), (d_2), (d_3)—at $J = 500$ A/cm^2; (e_1), (e_2), (e_3)—at $J = 650$ A/cm^2; (a_2, b_2, c_2, d_2, e_2) is a magnified image of (a_1, b_1, c_1, d_1, e_1), and (a_3, b_3, c_3, d_3, e_3) is a magnified image of (a_2, b_2, c_2, d_2, e_2)

and oxidized wear regions with an open-pore structure along the sliding direction with electrical current, and the surface roughness of carbon strip under an electric current is significantly higher than that of carbon strip under no electric current. Moreover, the increase in current density results in more arc crater and open pores, the gradual decrease in the size of wear debris adhered to the wear scars, as well as the increase in the amount of wear particles due to the enhanced oxidation extent [20] (Fig. 2a_3–e_3). This may be due to that owing to the absence of the electric current, the wear layers generated between the carbon/copper pairs can easily maintain a dynamic state of balance. Consequently, only low-stress abrasive wear and fatigue wear occurred under non-current-carrying condition. By contrast, the worn surface of carbon strip under an electric current exhibits thermal expansion [21], fatigue peeling and arc erosion phenomena, which would facilitate the generation of small wear debris. Moreover, the active sites of carbon on the worn surface are easily oxidized by thermal effects of arcing [8], which inevitably leads to the loosening of granules or coking of agglomerates. The higher the current density, the higher the degree of oxidation of carbon materials, which facilitates the formation of an open-pore structure in wear scar areas. This is consistent with the increase in the wear rate described in Sect. 3.1.

According to these observations, a typical wear scar area consists of ablation scars, arc craters and non-peeling wear debris under combined arcing and sliding friction. The results indicate that the tribological behavior under continuous arcing conditions is due to the interaction between arc erosion wear and oxidative wear, as well as fatigue peeling.

3.2.2 *Characterization of the Wear Debris*

The wear debris delaminated from the worn surface plays a key role in research on friction processes. Figure 3 shows the SEM morphologies of the wear debris of carbon contact strip under the electric current density of 0, 250, 375, 500 and 650 A/cm^2.

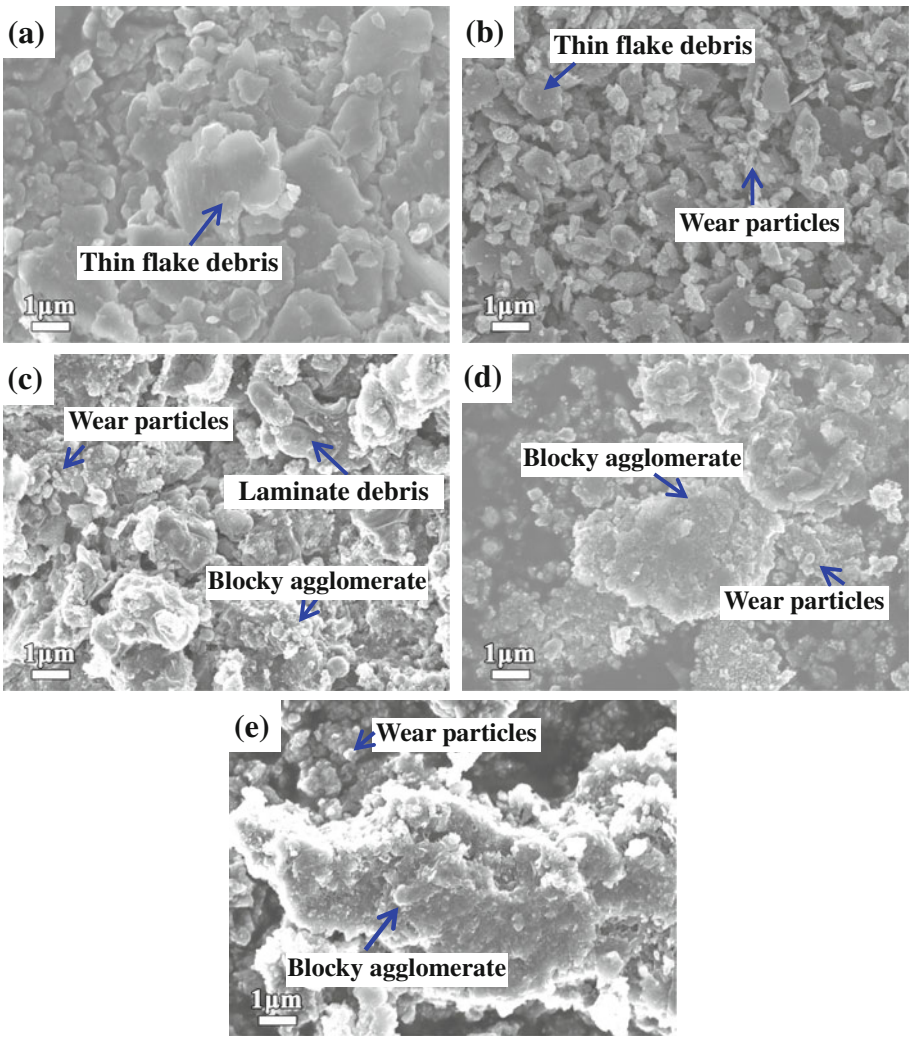

Fig. 3 SEM morphologies of the wear debris of carbon contact strip under electric current density: **a** at $J = 0$ A/cm^2; **b** at $J = 250$ A/cm^2; **c** at $J = 375$ A/cm^2; **d** at $J = 500$ A/cm^2; **e** at $J = 650$ A/cm^2

Figure 3 shows a significant difference between the morphologies of the wear debris produced at different current densities. As shown in Fig. 3a, the wear debris presents a typical morphology featuring irregular thin flakes when there is no current, and there are few spherical particles observed. However, during the current-carrier friction, the amount of wear particles gradually increases, as well as the size of the flake wear debris decreases. Furthermore, as the electric current density increases, the particles coalesce into larger blocky agglomerates and the size of the laminate debris increases (Fig. 3b–e). As mentioned in Sect. 3.2.1, this is attributed to the fact that the asperities on the wear scars of the carbon strip are shear-fractured and ground during the wear process, which directly leads to the detachment of wear particles from the contact interface. These observations clearly indicate that the thin-flake wear debris gradually transforms into granular structures, agglomerates and blocks with the increase in electric current density.

3.3 Effects of Electric Current Density on the Raman Spectra of the Wear Scars

The Raman spectra of corresponding wear scar samples under different electric current density are shown in Fig. 4. As shown in the figure, the main peaks [22] of all of the wear scar samples occur at similar positions, i.e., the G-band (a characteristic feature of the relative motion of sp^2 carbon atoms [23]) occurs at approximately 1,580 cm^{-1} and the D-band (a typical feature of defective graphitic structures) occurs at approximately 1,360 cm^{-1}. The intensity ratio of the D-band and G-band of the Raman signal, referred to as the R value ($R = I_D/I_G$), introduced by Tuinstra and Koenig [24], is listed in Table 1 for each sample. The R value was used to evaluate the effective crystallite size in the direction of the graphite plane (L_a). The increase in I_D/I_G intensity ratio corresponds to the decrease in the average crystallite size of sp^2-bonded clusters in the stage from graphite to nanocrystalline graphite [23]. In addition, L_a increases when there is a rise in the ordered degree [25]. Thus, to some extent, the peak intensity ratio of R (I_D/I_G) can represent the degree of graphitization [26], and the value of R is inversely proportional to the degree of graphitization [27]. Table 1 shows that the degree of graphitization of carbon in the wear scar areas first increases ($I < 500$ A/cm^2) and then decreases ($I > 500$ A/cm^2). In addition, the G-band intensities in the Raman spectra are higher than those of the D-band at 0, 250, 375 and 500 A/cm^2 in the wear scar areas, and the widths of the G-band are narrower than those of the D-band. This is mainly because the frictional heat and Joule heat, as well as the arc heat between the carbon/copper pairs when the current density is within 500 A/cm^2, provide enough energy to transform the texture and structure of the crystallites, which results in the increase in the degree of graphitization in the crystalline regions of the wear scar areas. However, the graphitic crystallites of the wear scars of carbon strip were destroyed as a result of oxidation and ablation under arcing conditions when the current density was 650 A/cm^2.

3.4 TEM Investigation of the Wear Debris

TEM images, high-resolution transmission electron microscopy (HRTEM) images and the corresponding fast Fourier transform (FFT) images of the carbon matrix and the wear debris under current density of 500 and 650 A/cm^2 are shown in Fig. 5.

The TEM images in Fig. 5 show clear differences between the carbon matrix and the two types of wear debris. Figure 5a_1 exhibits a preferred orientation of the graphitic crystallites in the carbon matrix, and there are no significant hallmarks of oxidation wear in the morphology. Novel entwined turbostratic carbon nanospheres (ETCNs), which have a similar structural characteristic to the carbon nanospheres prepared by rolling [28, 29], chemical vapor

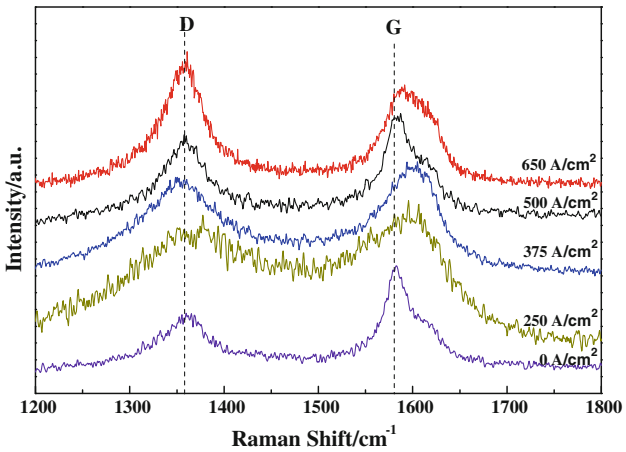

Fig. 4 Raman spectra of the wear scar areas of carbon strip under an electric current density

Table 1 Raman spectra data obtained in the wear scar areas of carbon strip

Areas	Current density/A/cm^2	D/cm^{-1}	G/cm^{-1}	R	1/R
Wear scar areas	0	1,360.93	1,591.54	1.28	0.78
	250	1,357.93	1,587.04	0.84	1.19
	375	1,350.43	1,605.05	0.88	1.13
	500	1,359.93	1,582.54	0.60	1.67
	650	1,377.44	1,595.55	0.92	1.09

deposition [30] and arc discharge [31], were clearly observed with a sphere-like stacking in the morphologies of wear debris of the carbon strip produced during the friction process with current (Fig. 5b, c). Besides, we can find that the higher the applied electric current density, the greater the number and size of ETCNs, by comparing Fig. 5b, c.

In order to acquire a better understanding of the ETCNs, HRTEM images and the corresponding FFT images of ETCNs were shown. Compared to the structure of the carbon matrix (Fig. 5a$_1$), the ETCNs exhibit a texture composed of organized curved-crystalline regions interspersed with texture-less regions, which show a structure of scrolled graphene layers (Fig. 5b$_1$, c$_1$). This discrepancy indicates that the degree of preferred orientation within the wear debris is clearly reduced and the intertwined texture is produced mainly due to the thermal effects of arcing, which may be one of the reasons for the severe wear of the carbon strip [32]. The formation mechanism of ETCN is similar to that of corannulene-like carbon structures [29, 33, 34]. First, the crystallite regions in areas of arc erosion

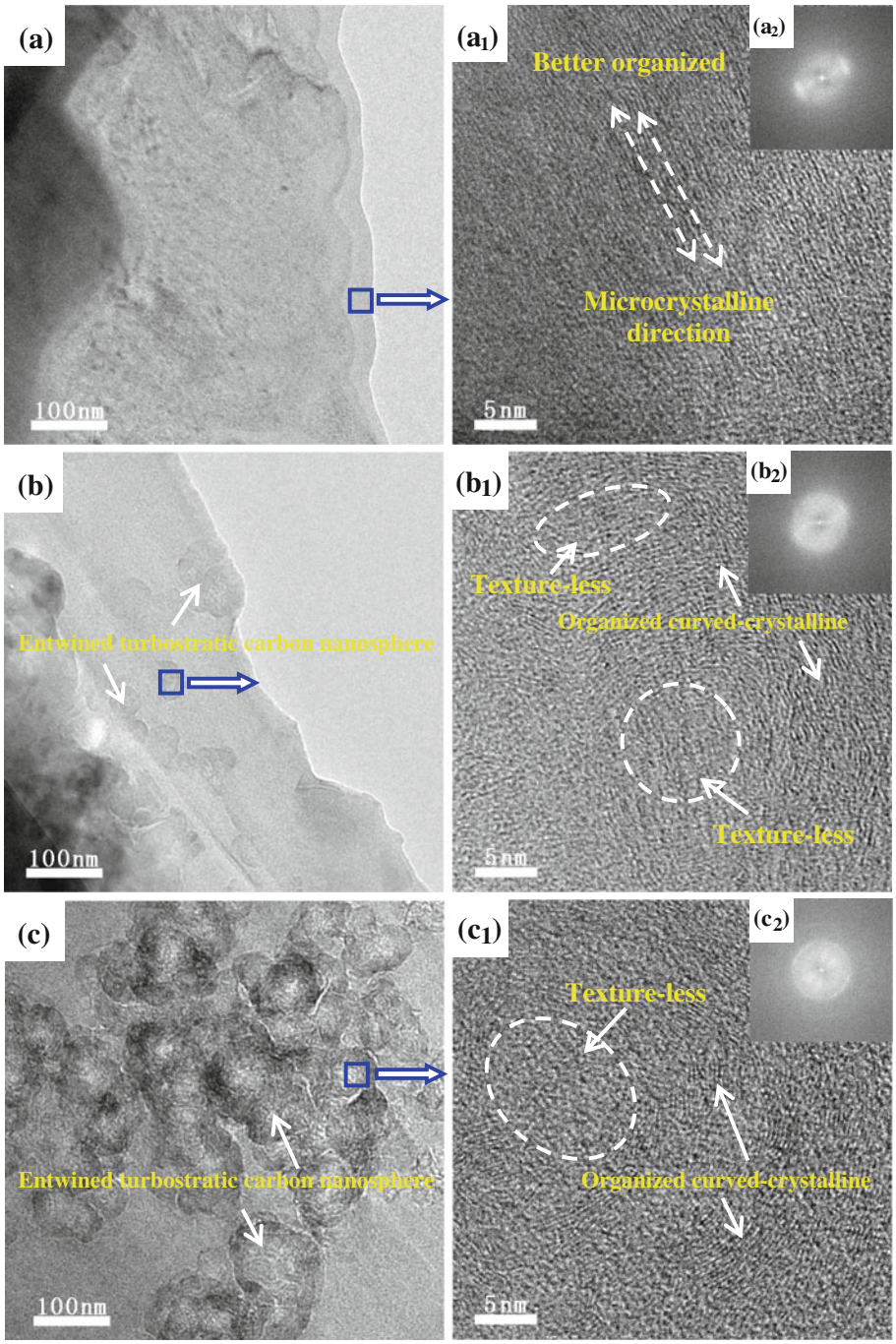

Fig. 5 TEM images and corresponding FFT images: **a**, **b**, **c** TEM images of the carbon matrix, the wear debris at $J = 500$ A/cm^2 and the wear debris at $J = 650$ A/cm^2; a_1, b_1, c_1 HRTEM images of the carbon matrix, the wear debris at $J = 500$ A/cm^2 and the wear debris at $J = 650$ A/cm^2; a_2, b$_2$, c$_2$ FFT images of a$_1$, b$_1$, c$_1$

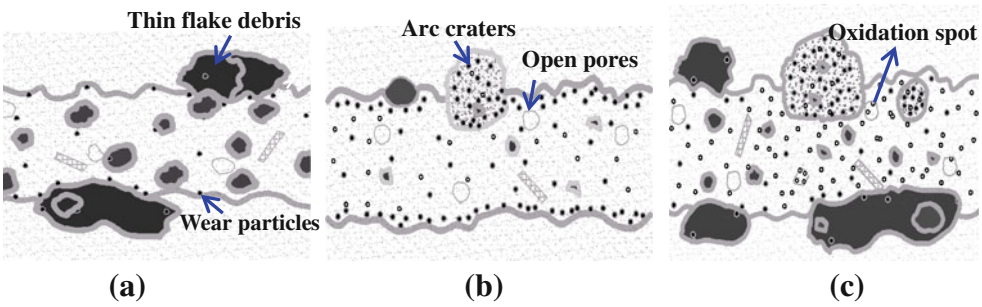

Fig. 6 State of the worn surface of carbon strip: **a** without electrical current, **b** at $J = 500$ A/cm^2, **c** at $J = 650$ A/cm^2

become texture-less due to the high temperature instantly induced by arcing, which directly leads to changes in textural features, and the structure of the better-organized crystalline regions is converted to texture-less to counteract the arc ablation. Second, due to the different extents of heating expansion of the carbon layers on wear scars at high temperature and stress, the crystalline states of the carbon layers are altered and rearranged, causing the ETCNs to curvature and deform [28]. The numerous sphere-like stacks composed of texture-less regions/organized curved-crystalline regions are formed by high-temperature electric arcing. The heat generated from the arc discharge directly leads to the abscission and heat damage of the wear debris, and the ETCNs are formed easily to reduce the surface free energy by bending and rearranging the carbon layers. In addition, the variation in the (002) diffraction arc shown in Fig. 5 is consistent with change in the texture of the crystalline states based on the FFT images of the entire field of view [35]. The study shows that the formation of ETCNs is closely related to the arc discharge; however, to better understand the formation mechanisms and the effects to the wear process, further study is required.

3.5 Arc Erosion Wear Mechanisms of the Carbon/Copper Pair

Figure 6 shows the state of the worn surface of carbon strip, which is simulated from the SEM morphologies of the worn surfaces (Fig. 2). The discussion of Arc erosion wear mechanisms of the carbon/copper pair is based on the observations and analysis above.

Figure 6a shows that a few wear fragments in the form of thin flakes were produced during mechanical wear testing in the absence of an electrical current. These flakes were attached to the interfaces of the carbon/copper pair to effectively prevent the friction pairs from making direct contact. As a result, the model of purely mechanical wear mainly includes low-stress abrasive particle wear and fatigue wear, as well as mild adhesive wear. However, during the friction process with current, it is now generally accepted that the oxidation and gasification around the arcing area are easily induced by arcing [8, 9, 17]. Therefore, a portion of carbon material is lost by sublimation and oxidation [14, 36]. As expected, arc craters are found as shown in Fig. 6b, c. While it should be noted that the increase in electrical intensity activates the oxidation process at the interface [10, 37], as mentioned in Sect. 3.1, the carbon strip would directly oxidized in an oxidizing atmosphere when the worn surface is overheated.

In short, it can be concluded that the arc erosion wear mechanisms of carbon strip sliding against copper under continuous arcing conditions are mainly due to the synergetic action of oxidation ablation, local electric arc impact and high-temperature graphitization.

4 Conclusions

To obtain a comprehensive understanding of the arc erosion wear characteristics and mechanisms of pure carbon strip against copper under continuous arcing conditions, detailed wear testing and structural characterization were performed. The microstructure of the carbon material turns into low texture under continuous arcing conditions. Typical entwined turbostratic carbon nanospheres exhibiting sphere-like stacking structure were found in the microstructure of wear debris of the carbon strip under the interaction of arcing and sliding friction; these bodies were different from those found in the carbon matrix. In addition, the number and size of ETCNs increase under higher electric current density. A combination behavior of arc erosion wear and oxidative wear, as well as fatigue peeling, is the dominant wear mechanism of pure carbon strip against copper during the electrical sliding wear process. The arc erosion wear mechanisms of pure carbon strip against copper are mainly due to the synergetic action of oxidation ablation, local electric arc impact and high-temperature graphitization under continuous arcing.

Acknowledgments This work is supported by the National Natural Science Foundation of China (51102089, 51171063), the National Basic Research (973) Program of China (2009CB623704), the China

Postdoctoral Science Foundation (2011 M500127), the Hunan Provincial Natural Science Foundation of China (12JJ4046, 12JJ9014) and the Science Foundation for the Excellent, Youth Scholars of Hunan University.

References

1. Jia, S.G., Liu, P., Ren, F.Z., Tian, B.H., Zheng, M.S., Zhou, G.S.: Sliding wear behavior of copper alloy contact wire against copper-based strip for high-speed electrified railways. Wear **262**, 772–777 (2007)
2. Yang, H.J., Chen, G.X., Zhang, S.D., Zhang, W.H.: Effect of the vibration on friction and wear behavior between the carbon strip and copper contact wire pair. Proc Inst Mech Eng J **226**, 722–728 (2012)
3. Giuseppe, B., Andrea, C.: A procedure for the wear prediction of collector strip and contact wire in pantograph-catenary system. Wear **266**, 46–59 (2009)
4. Zhou, N., Zhang, W.H.: Investigation on dynamic performance and parameter optimization design of pantograph and catenary system. Finite Elem Anal Des **47**, 288–295 (2011)
5. He, D.H., Manory, R., Sinkis, H.: A sliding wear tester for overhead wires and current collectors in light rail systems. Wear **239**, 10–20 (2000)
6. Tu, C.J., Chen, D., Xia, J.T.: Improving the tribological behavior of graphite/Cu matrix self-lubricating composite contact strip by electroplating Zn on graphite. Tribol Lett **31**, 91–98 (2008)
7. Matsuyama, S.: Electric contact tribological behavior of pantograph. Toyo Denki Giho **91**, 52–60 (1995)
8. Kubo, S., Kato, K.: Effect of arc discharge on the wear rate and wear mode of a copper impregnated metallized carbon contact strip sliding against a copper disk. Tribol Int **32**, 367–378 (1999)
9. Kubo, S., Kato, K.: Effect of arc discharge on wear rate of Cu-impregnated carbon strip in unlubricated sliding against Cu trolley under electric current. Wear **216**, 172–178 (1998)
10. Senouci, A., Zaidi, H., Frene, J., Bouchoucha, A., Paulmier, D.: Damage of surfaces in sliding electrical contact copper/steel. Appl Surf Sci **144**(145), 287–291 (1999)
11. Nagasawa, H., Kato, K.: Wear mechanism of copper alloy wire sliding against iron-base strip under electric current. Wear **216**, 179–183 (1998)
12. Chen, Z.H., Tu, C.J., Chen, D., Xia, J.T., Yan, H.G.: Preparation and tribological investigation of resin binder contact strip with variable current. Mater Sci Technol **25**, 607–613 (2009)
13. Ding, T., Chen, G.X., Wang, X., Zhu, M.H., Zhang, W.H., Zhou, Z.R.: Friction and wear behavior of pure carbon strip sliding against copper contact wire under AC passage at high speeds. Tribol Int **44**, 437–444 (2011)
14. Tu, C.J., Chen, Z.H., Xia, J.T.: Thermal wear and electrical sliding wear behaviors of the polyimide modified polymer-matrix pantograph contact strip. Tribol Int **42**, 995–1003 (2009)
15. Ke, X., Bals, S., Romo Negreira, A., Hantschel, T., Bender, H., Van Tendeloo, G.: TEM sample preparation by FIB for carbon nanotube interconnects. Ultramicroscopy **109**, 1353–1359 (2009)
16. Ma, X.C., He, G.Q., He, D.H., Chen, C.S., Hu, Z.F.: Wear of railway contact wires against current collector materials. Wear **265**, 1087–1092 (2008)
17. Ding, T., Chen, G.X., Bu, J., Zhang, W.H.: Effect of temperature and arc discharge on friction and wear behaviours of carbon strip/copper contact wire in pantograph–catenary systems. Wear **271**, 1629–1636 (2011)
18. Lins, V.F.C., Cecconello, E.S., Matencio, T.: Effect of the current density on morphology, porosity, and tribological properties of electrodeposited nickel on copper. J Mater Eng Perform **17**, 741–745 (2008)
19. Qian, G., Feng, Y., Li, B., Huang, S.Y., Liu, H.J., Ding, K.W.: Effect of electrical current on the tribological behavior of the Cu-WS2-G composites in air and vacuum. Chin J Mech Eng **26**, 384–392 (2013)
20. Sahin, Y., Kilicli, V.: Abrasive wear behaviour of SiCp/Al alloy composite in comparison with ausferritic ductile iron. Wear **271**, 2766–2774 (2011)
21. Marshall, R.A.: The mechanism of current transfer in high current sliding contacts. Wear **37**, 233–240 (1976)
22. Lei, B.L., Yi, M.Z., Xu, H.J., Ran, L.P., Ge, Y.C., Peng, K.: Raman spectroscopy investigation of structural and textural change in C/C composites during braking. J Cent South Univ Technol **18**, 29–35 (2011)
23. Ferrari, A.C., Robertson, J.: Interpretation of Raman spectra of disordered and amorphous carbon. Phys Rev B **61**(20), 14095–14107 (2000)
24. Tuinstra, F., Koenig, J.L.: Raman spectrum of graphite. J Chem Phys **53**, 1126–1130 (1970)
25. Zhang, R.J., Wang, H., Li, Y.J.: Structures and high temperature friction and wear performances of Ti/Ni-doped carbonaceous mesophases. Tribol Lett **32**, 43–48 (2008)
26. Li, D.F., Yang, G.Z., Qi, L.N., Zheng, Q.B., Yang, J.H.: Raman study of the relationship between microstructure and physical properties of isotropic graphite. Adv Mater Res **487**, 860–863 (2012)
27. Yoshida, A., Kaburagi, Y., Hishiyama, Y.: Full width at half maximum intensity of the G band in the first order Raman spectrum of carbon material as a parameter for graphitization. Carbon **44**, 2333–2335 (2006)
28. Li, Z.Q., Lu, C.J., Xia, Z.P., Zhou, Y., Luo, Z.: X-ray diffraction patterns of graphite and turbostratic carbon. Carbon **45**, 1686–1695 (2007)
29. Li, J.L., Peng, Q.S., Bai, G.Z., Jiang, W.: Carbon scrolls produced by high energy ball milling of graphite. Carbon **43**, 2817–2833 (2005)
30. Chen, X.H., Deng, F.M., Wang, J.X., Yang, H.S., Wu, G.T., Zhang, X.B., Peng, J.C., Li, W.Z.: New method of carbon onion growth by radio-frequency plasma-enhanced chemical vapor deposition. Chem Phys Lett **336**, 201–204 (2001)
31. Qiao, W.M., Song, Y., Lim, S.Y., Hong, S.H., Yoon, S.H., Mochida, I., Imaoka, T.: Carbon nanospheres produced in an arc-discharge process. Carbon **44**, 187–190 (2006)
32. Kim, D.G., Kweon, D.W., Lee, J.Y.: The wear properties of carbon/carbon composites prepared by chemical vapour deposition. J Mater Sci Lett **12**, 8–10 (1993)
33. Dorin, V.P., Lawrence, T.S.: Addition of dihalocarbenes to corannulene. A fullerene-type reaction. Tetrahedron Lett **41**, 9633–9637 (2000)
34. Seiders, T.J., Baldridge, K.K., Grube, G.H., Siegel, J.S.: Structure/energy correlation of bowl depth and inversion barrier in corannulene derivatives: combined experimental and quantum mechanical analysis. J Am Chem Soc **123**, 517–525 (2001)
35. Wen, K.Y., Marrow, T.J., Marsden, B.J.: The microstructure of nuclear graphite binders. Carbon **46**, 62–71 (2008)
36. Gao, L., Jin, H.G., Liu, Z.L., Zheng, D.X.: Exergy analysis of coal-based polygeneration system for power and chemical production. Energy **29**, 2359–2371 (2004)
37. Han, J.C., He, X.D., Du, S.Y.: Oxidation and ablation of 3D carbon–carbon composite at up to 3000-degrees-C. Carbon **33**, 473–478 (1995)